Article:
Jones, NE, Burnett, CA, Salamon, S et al. (9 more authors) (2018) Fluoride doped γ-Fe_2O_3 nanoparticles with increased MRI relaxivity. Journal of Materials Chemistry B, 6 (22). pp. 3665-3673. ISSN 2050-750X

https://doi.org/10.1039/C8TB00360B

Fluoride Doped γ-Fe_2O_3 Nanoparticles with Increased MRI Relaxivity

N. E. Jones,[1] C. A. Burnett,[2] S. Salamon,[3] J. Landers,[3] H. Wende,[3] L. Lazzarini,[4] P. Gibbs,[5] M. Pickles,[5] B. Johnson,[6] D. J. Evans,[1] S. J. Archibald[1,8] and M. G. Francesconi[1*]

[1] School of Mathematics and Physical Sciences-Chemistry, University of Hull, Cottingham Road, Hull, HU6 7RX.

[2] Department of Chemistry, University of Warwick, Gibbet Hill, Coventry, CV4 7AL

[3]Faculty of Physics and Center for Nanointegration Duisburg-Essen (CENIDE), University of Duisburg-Essen, 47057 Duisburg, Germany

[4] IMEM-CNR Parco Area delle Scienze 37/A, 43124 Parma, Italy

[5] Centre for MR Investigation, University of Hull, Royal Infirmary, Anlaby Road, Hull HU3 2JZ

[6] School of Physics & Astronomy, E C Stoner Building, University of Leeds, Leeds, LS2 9JT.

[8]Positron Emission Tomography Research Centre, University of Hull, Cottingham Road, Hull, HU6 7RX.

Abstract

Iron oxide nanoparticles (IONs) are being actively researched and experimented as contrast agents for Magnetic Resonance Imaging (MRI), as well as image-directed delivery of therapeutics. The efficiency of an MRI contrast agent can be described by its longitudinal and transverse relaxivities, r_1 and r_2. γ-Fe_2O_3 nanoparticles - doped with fluoride in a controlled manner and functionalised with citric acid - showed a 3-fold increase in r_1 and a 17-fold increase in r_2 in a magnetic field of 3 T and almost 6-fold increase in r_1 and a 14-fold increase in r_2 at 11 T. Following fluorination, PXRD shows that the crystal structure of γ-Fe_2O_3 is maintained, Mössbauer spectroscopy shows that the oxidation state of the Fe cation is unchanged and HREM shows that the particle size does not vary. However, magnetisation curves show a large increase in the coercive field, pointing towards a large increase in the magnetic anisotropy for the fluorinated nanoparticles compared to the un-doped γ-Fe_2O_3 nanoparticles. Therefore, a chemically induced increase in magnetic anisotropy appears to be the most relevant parameter responsible for the large increase in relaxivity for γ-Fe_2O_3 nanoparticles.

Introduction

Iron oxide nanoparticles (IONs) are becoming increasingly popular for use in biomedical applications such as magnetic resonance imaging (MRI) for the detection of diseased tissues, as well as image-directed delivery of therapeutics.[1,2] For example, low concentration biomarkers can be difficult to detect because of the limited sensitivity of the MRI equipment, however, the signal intensity of MRI can be improved by introducing contrast agents. IONs are being heavily investigated for their potential as MRI contrast agents due to their high biocompatibility in comparison to other magnetic compounds, their high magnetic moment, low toxicity and wide availability. Moreover, IONs can be directed specifically to the in vivo target through the modification of their surfaces with specific binding groups that interact with the target tissue.[3] Several formulations based on IONs have already received approval by FDA for clinical trial, mainly to be used as MRI contrast agents.[1] Many current studies are directed towards increasing the magnetic performance of IONs, so that lower doses of nanoparticles will need to be injected in the patient's body. The signal recorded during an MRI scan relates to magnetic relaxation processes occurring for the nucleai of the proton of the water molecules in the area of the body, hence the efficiency of a contrast agent is usually described using relaxivities, r_i (i = 1, 2). The longitudinal (r_1) and transverse (r_2) relaxivities are defined as the relaxation rate per unit concentration ($mmol \times L^{-1}$) of magnetic cation and are connected to the efficacy of contrast enhancement, i.e. quality of images. The Koenig-Keller model relates the relaxivities to the magnetic moment of the nanoparticles.[4] Considering that, in inorganic solids, there is a direct link between the magnetic properties and the chemical composition, the efficiency of inorganic nanoparticles as contrast agent to enhance contrast for higher quality images, is directly correlated with their chemical composition, as well as the particle size, surface properties and functionalisation. Hence, it is crucial to design nanoparticles with tuneable magnetic properties and surface functionalisation to obtain optimum MRI contrast. Fine adjustment of the chemical composition via doping is one well established tool to modify and fine tune magnetic properties in inorganic solids.[5]

Several iron oxides are available in nature and can be prepared in chemistry lab but the acronym IONs, generally refers, mainly, to magnetite (Fe_3O_4) and to the more stable maghemite (γ-Fe_2O_3), as both iron oxides show magnetic moment of appropriate intensity.[5]

The crystal structures of magnetite (Fe_3O_4) and maghemite (γ-Fe_2O_3) are very similar, both based on a FCC lattice of O^{2-} anions. In Fe_3O_4 Fe^{2+} is located in the octahedral holes and Fe^{3+}

in both the octahedral and tetrahedral holes. In γ-Fe_2O_3 all Fe cations show oxidation state +3 and are randomly distributed between octahedral and tetrahedral holes. As both structures are based on an FCC lattice, Fe_3O_4 can be interconverted into γ-Fe_2O_3 via oxidation and consequent creation of cation vacancies. Fe_3O_4 is frequently non-stoichiometric ($Fe_{3-x}O_4$) and has been found to oxidise easily into a series of intermediates with varying content of Fe^{2+} (magnetite-magnemite solid solution).[6]

So far cationic substitution/insertion reactions have assured progress in the modification of chemical formulas of inorganic solids and discovery of new materials, and are expected to continue to do so. Particularly, cobalt, nickel, and manganese doped Fe_3O_4 nanoparticles, MFe_2O_4 (M = Co, Mn, Ni, Zn) nanoparticles of size 35–50 nm were reported to be potential alternatives to IONs due to their superparamagnetism at room temperature, high saturation magnetization, high surface area, high density of surface amine groups and good aqueous dispersion stability.[7,8,9] However, manipulation of the anion population of inorganic solids has been pursued less due, mainly, to experimental challenges. Despite this limitation, structural and electronic modifications through alteration of the anionic makeup has yielded several interesting compounds in recent years, due to the larger differences in nature, size, charge and electronegativity seen with non-metals, when compared with metals. In addition, when different anions coexist in the same structure an eclectic mix of bonding types and coordination environments for the cations are present and, often, unique structures can be created.[10] In particular, the partial replacement of oxide anions with fluoride anions has been widely researched for the modification of electronic properties in advanced materials such as superconductors.[11]

There are only a handful of published examples of fluorination of iron oxides. The action of fluorine on iron oxides was investigated in 1974. The fluorination of a crystal of Fe_2O_3 (it is not specified whether the γ- Fe_2O_3 or the α-Fe_2O_3 polymorph was used) with F_2 or HF led to no reaction for temperatures T < 300 °C and formation of FeF_3 on the surface for T ≥ 300 °C. [12] More recently, Fe_3O_4 nanoparticles were fluorinated to improve their performance as cathodes in Li-ion batteries. Firstly, Fe_3O_4 nanoparticles were reacted with F_2 gas in a fluidised bed reactor and surface formation of FeOF was found for reaction temperatures T ≥ 100 °C.[13] Direct fluorination under fluorine gas using a fluidized bed reactor was also performed on γ-Fe_2O_3 nanoparticles. At reaction temperatures below 250 °C, surface fluorination was obtained and a phase of general composition $Fe_2O_{3-x}F_{2x}$ (x < 1) was obtained. At fluorination

temperature $T \geq 275$ °C, interconnected nano-domains of FeF_3 and Fe_2O_3 were found to coexist in the same nanoparticles.[14]

^{18}F is well known as a radiolabelling agent for use with imaging techniques such as positron emission tomography (PET) and therefore development of a fluorine modified iron oxide nanoparticle could have potential as a dual MRI/PET probe.[15] There have also been exciting advances in the area of direct nanoparticle radiolabelling to offer the incorporation of radioisotopes in stable one-step processes.[16,17,18] The combination of stable fluoride containing materials into this process offers a further opportunity for new multimodal probes.[19] MRI/PET is a developing imaging modality combination that is growing in clinical relevance and there is a desire to develop applications and agents for new clinical imaging procedures.[20, 21]

In this work, we performed a partial substitution of fluoride anions for oxide anions in γ- Fe_2O_3 nanoparticles using an experimentally simple and low-cost reaction.[22, 23] The application of IONs as MRI contrast agents rely on the magnetic properties of these oxides, hence phase purity is of paramount importance to ensure repeatability and consistent performance. We focused on γ-Fe_2O_3 nanoparticles and not on Fe_3O_4 nanoparticles to be certain of fluorinating single phase samples. The most interesting outcome of this work is that the crystal structure and magnetic moment do not change following fluorination, instead there is a large increase in the coercive field and magnetic anisotropy. This increase seems to be responsible for the higher relaxivity shown by the fluorinated γ-Fe_2O_3 nanoparticles.

Experimental

0.01045 moles of $FeCl_2.4H_2O$ and 0.0209 moles of $FeCl_3$ were mixed in 50 mL ethylene glycol and heated to 80˚C. 5M NaOH solution was added dropwise until the pH of the solution reached 10. The temperature was then increased to 120˚C and the solution stirred. After 1 hour, the heat was removed. The mixed solution was exposed to an oxygen rich atmosphere by connecting a separate flask of decomposing H_2O_2 (30%, 100 volumes; 25 mL) to the main reaction vessel and left overnight. The nanoparticles were collected magnetically and washed with warm water before being dried in an oven.

0.5g of the prepared γ-Fe_2O_3 was thoroughly ground with a pestle in a mortar at a 1:1 molar ratio with NH_4F powder and heated at 250˚C for 8 hours in air. The grinding process was carried out for at least 15 minutes to insure homogeneity of the reaction mixture.

Powder X-Ray diffraction patterns were collected on a Siemens D5000 Diffractometer with Cu $K_{\alpha 1}$ radiation (1.54 Å) at 30 mA, 40 kV with a step size of 0.02 degrees 2 theta and a 0.5 ° fixed divergence slit.

The TEM investigations have been carried out in a JEOL 2200FS field emission microscope operated at 200kV, with point-to-point resolution 0.185 nm (0.136 nm in STEM mode), equipped with in-column filter, X-ray microanalysis, and two high angle annular dark field (HAADF) detectors for chemical imaging. The so called HAADF-STEM technique is also known as Z contrast, as, in the proper conditions, the dominant mechanism in the images is represented by the differences of the mean atomic number.

The powder are dispersed in isopropanol, sonicated and then dropped on holey carbon grids for the observation.

Mössbauer spectra were recorded in transmission geometry using a ^{57}Co source mounted on a Mössbauer drive operating in constant-acceleration mode. Low temperature in-field measurement were performed in a liquid helium bath cryostat, using a superconducting split-pair magnet to apply a homogenous field of 5T at the sample position.

M(H) curves were recorded with the vibrating sample magnetometer (VSM) option of a Quantum Design PPMS DynaCool, while M(T) measurements were performed with a Quantum Design MPMS-5S.

XPS measurements were performed using a VG Escalab 250 XPS with monochromated aluminium K-alpha X-ray source. The samples were mounted onto carbon tape for analysis. The spot size was 500 μm with a power of 150W. Detailed spectra of individual peaks were taken at energy of 20 eV with a step size of 0.1 eV. Detailed spectra had a Shirley or linear background fitted to them and peaks were fitted and deconvoluted using mixed Gaussian-Lorentzian fits (using CASAXPS). Any shift in the spectra was corrected for using the carbon peak at 285 eV.

The nanoparticles were dispersed in an aqueous solution of citric acid in a 1:1.2 $Fe_2O_{3-x}F_x$: citric acid molar ratio. Hydrochloric acid was added until the solution reached pH 4. The mixture was stirred for 2 hours before magnetic decantation and the collected nanoparticles were washed with deionised water and the pH adjusted to pH 7 by adding a 5M solution of NaOH. These solutions were then used for MRI and NMR measurements.

Hydrodynamic radii of the functionalised nanoparticles were measured using Nanosight LM10 with Nanoparticle Tracking Analysis (NTA) Version 2.3 Build 0011 RC1. Analysis settings: Frames per Second: 23.22, Calibration: 186 nm/pixel, Blur: Auto, Detection Threshold: 10 Multi, Min Track Length: Auto, Min Expected Size: 100 nm, Temperature: 22.00 ^{o}C, Viscosity: 0.95 cP.

Relaxivity measurements were collected at 3 T and 11.7 T magnetic field strength. Relaxivity data were collected at 3 T using a 3.0 T (Discovery 750) GE scanner. T2 weighted images (for R2 quantification) were acquired using a spin-echo imaging sequence with the following parameters: TR 600 ms, slice thickness 5 mm, field of view 24×19.2 cm with 256×256 matrix size (image resolution is thus 0.94 mm by 0.75 mm), acquisition time 2 mins 12 secs. Repeated for 10 different echo-times (10, 15, 20, 25, 30, 35, 40, 50, 70, 100 ms) for a total acquisition time of 22 minutes. R2 was quantified via simplex minimisation using:

$$S=S_o e^{-TEXR2}$$

T1 weighted images (for R1 quantification) were acquired using an inversion recovery imaging sequence with the following parameters: TR 6000 ms, TE 12.1 ms, slice thickness 5 mm, field of view 24×19.2 cm with 256×256 matrix size (image resolution is thus 0.94 mm by 0.75 mm), acquisition time 2 mins 6 secs. Repeated for 10 different inversion times (50, 100, 200, 300, 400, 500, 600, 800, 1000, 1500 ms) for a total acquisition time of 21 minutes. R1 quantified via simplex minimisation using:

$$S=S_0(1-2e^{-T1XR1})$$

Relaxivity measurements at 11.7 T magnetic field strength were collected using a Bruker 500 MHz NMR. For T1 relaxation study, FISP T1 + T2 map sequence protocol was used with used parameters: FOV = 4.0 cm, FA = 60 dg, TR = 3.0 ms, TE = 1.5 ms, TA = 5 min 20 s, T1 = 65 ms. T2 relaxivity data was collected using a MSME sequence protocol (Bruker MSME-T2-map) where FOV = 4.0 cm, FA = 180 dg, TR = 2000 ms, TE = 10 ms, TA = 6 min 24 s.

For the phantom measurements, aqueous suspensions were prepared at different concentrations (between 100 µM and 500 µM).

Results and Discussion

Steps were taken during the synthesis of the starting iron oxide to achieve single-phase samples of γ-Fe_2O_3. Specifically, the oxidising agent H_2O_2 was added to make sure that all Fe^{2+} was oxidised to Fe^{3+} or, in other words, that all Fe_3O_4 formed initially would be transformed into γ-Fe_2O_3. To ascertain that the sample was single-phase γ-Fe_2O_3, the PXRD data for γ-Fe_2O_3

were analysed using a peak deconvolution method that allows calculations of the percentage of Fe_3O_4 and γ-Fe_2O_3 in nanocrystalline samples.[24] The (440) diffraction peak was used for the deconvolution and the resulting weight percentages, 98.5 % for γ-Fe_2O_3 and 1.5% for Fe_3O_4, led to the conclusion that the iron oxide samples prepared in this work can be reasonably approximated to single-phase γ-Fe_2O_3 samples.

The fluorination reaction was performed using the solid fluorinating agent NH_4F. The fluorination reaction with NH_4F is classified as a "soft-chemistry" reaction due to the fact that it is usually carried out at a relatively low temperature (100 – 250 °C). This method has been vastly used for the fluorination of oxides and was reported to occur via the decomposition of NH_4F into NH_3 and HF, which then reacts with the oxide.[22]

The fluorination reaction was attempted also using higher amounts of NH_4F, specifically using the following NH_4F : γ-Fe_2O_3 molar ratios: 1:1, 2:1 and 3:1. However, reactions involving NH_4F : γ-Fe_2O_3 molar ratios higher than 1:1 led to increasing amount of α-Fe_2O_3 (hematite) as secondary phase. The amount of the secondary phase seemed to increase with the increasing NH_4F : γ-Fe_2O_3 molar ratio.

Both PXRD patterns of the fluorinated and un-doped γ-Fe_2O_3 (Figure 1) show the same set of peaks with no detectable 2 theta shift and no detectable peaks corresponding to impurities, although amorphous impurities cannot be completely excluded. This shows that the fluorinated compound maintains the maghemite structure of the starting material.

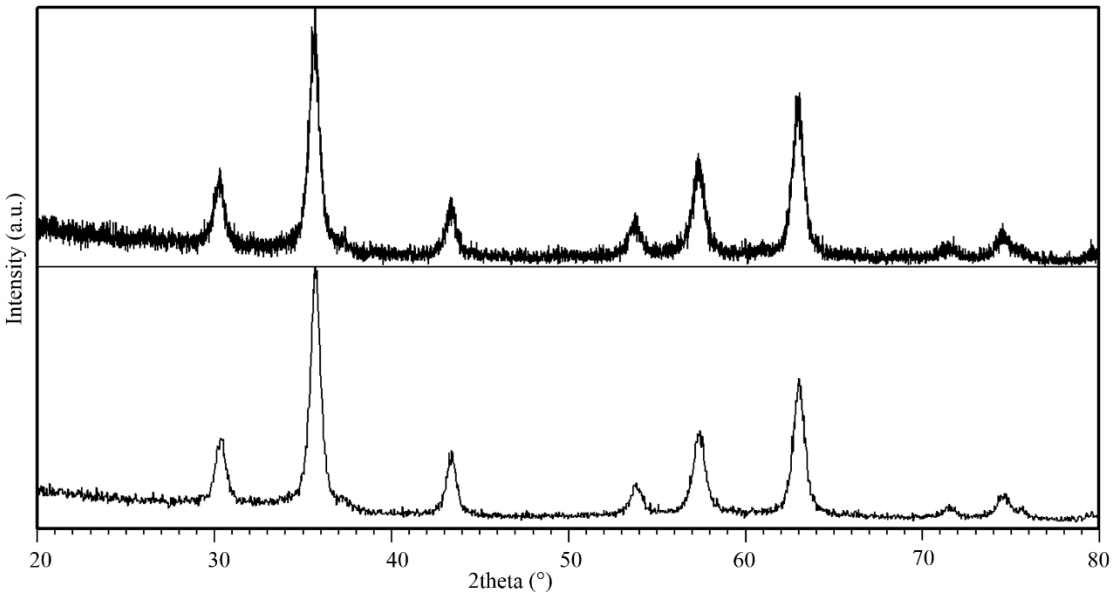

Figure 1- PXRD patterns for γ-Fe_2O_3 nanoparticles (bottom) and γ-Fe_2O_3 fluorinated nanoparticles (top).

The unit cell parameters of γ-Fe_2O_3, and fluorinated γ-Fe_2O_3, were calculated using the model reported by Pecharroman et al. ($Fd\bar{3}m$, a = 8.33 Å) and found to be a = 8.344(2) Å, and a = 8.355(1) Å respectively, revealing a small increase in the lattice parameter of the doped γ-Fe_2O_3 nanoparticles.[25]

The XPS spectrum (Figure 2a) of the γ-Fe_2O_3 sample shows three peaks corresponding to Fe (~709 eV) and a peak corresponding to O^{2-} (~529 eV). The peak at 285 eV can be assigned to carbon and the peaks at 785 and 495 eV can be assigned to an Fe auger and Na auger, respectively.[26]

(a)

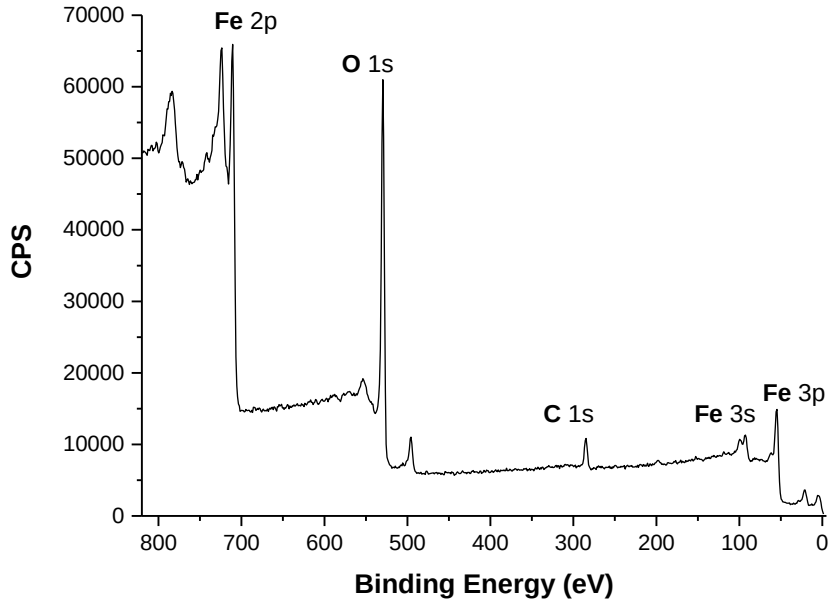

(b)

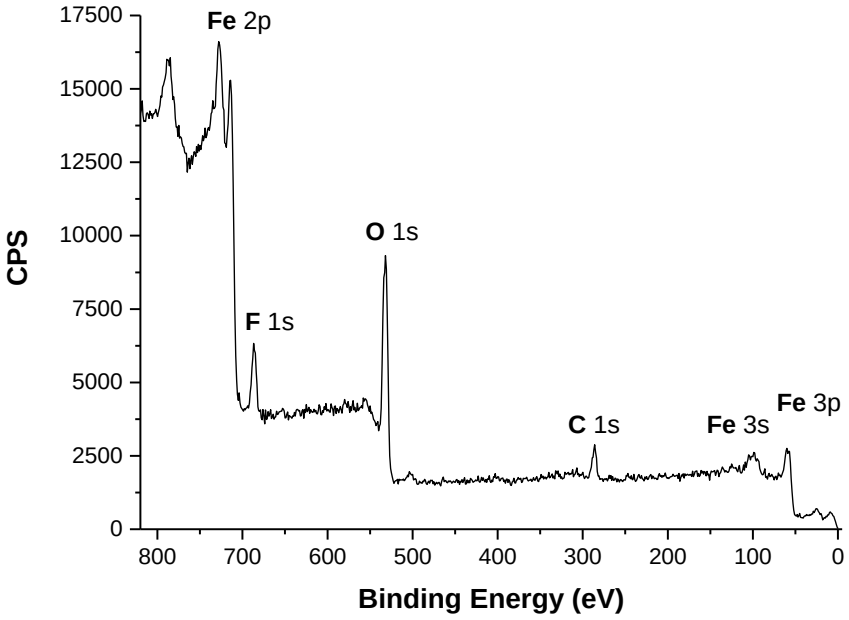
17500
15000
12500
10000
7500
5000
2500
0
CPS
Fe 2p
O 1s
F 1s
C 1s
Fe 3s
Fe 3p
800
700
600
500
400
300
200
100
0
Binding Energy (eV)

(c)

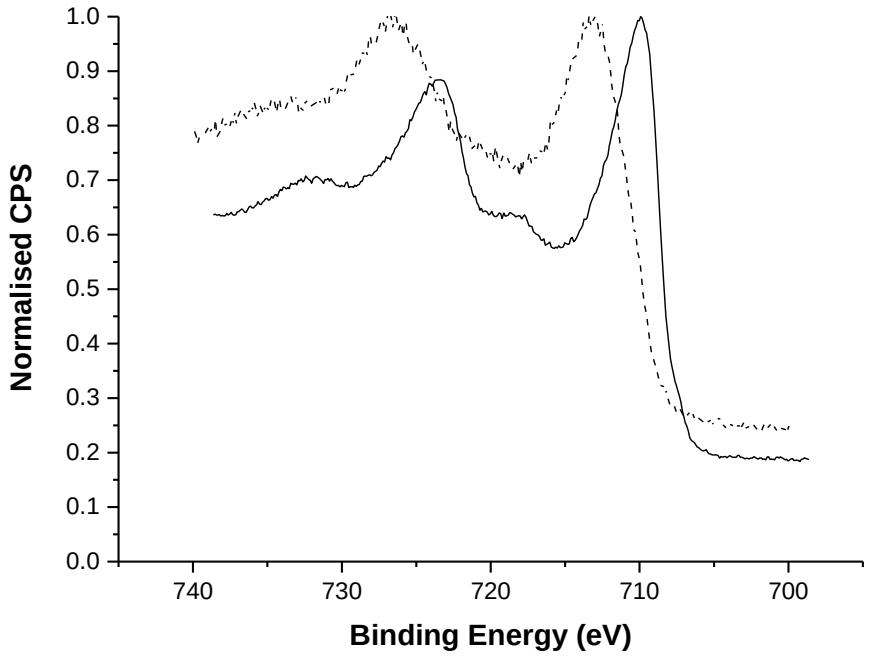

Figure 2- XPS survey spectra for (a) the prepared iron oxide nanoparticles; (b) the prepared fluorinated iron oxide nanoparticles. (c) XPS spectrum of Fe 2p peaks for γ-Fe_2O_3 nanoparticles (solid line) and fluorinated iron oxide nanoparticles (dashed line).

The XPS spectrum for the fluorinated γ-Fe_2O_3 sample (Figure 2b) confirms the presence of fluorine, with the F1s peak at 686.93 eV. Quantitative data on anion and cation atomic percentages were also obtained and are listed in Table 1.

Table 1. Atomic percentages determined by XPS.

Sample	Fe 2p (%)	O (%)	F (%)
γ-Fe_2O_3	30.8	69.2	0.0
1:1 NH_4F:Fe_2O_3	26.9	53.1	20

Figure 2c shows the enlarged sections of the XPS spectra of γ-Fe_2O_3 and fluorinated γ-Fe_2O_3. The peaks observed relate to Fe 2p 3/2 and Fe 2p 1/2 and their satellites. From visual comparison of the two spectra, it can be seen that the XPS spectrum of the fluorinated γ-Fe_2O_3 is shifted to higher binding energies. This indicates changes in bonding, possibly due to the

presence of the more electronegative fluoride anion. In fact, it was reported by Grosvenor et al. that the more ionic the Fe-ligand bond the higher the binding energy.[27]

Considering that the PXRD pattern does not show any peaks corresponding to secondary phases it is reasonable to assume that fluoride doping of γ-Fe_2O_3 has occurred and an oxide-fluoride was formed. It is difficult, at this preliminary stage, to clarify whether the doping occurred via insertion of fluoride anions ($Fe_2O_3F_x$), substitution of two fluoride anions for one oxide anion ($Fe_2O_{3-x}F_{2x}$) or substitution of one fluoride for one oxide anion ($Fe_2O_{3-x}F_x$). It can be safely said that it is unlikely that the doping mechanism is insertion of a fluoride anion ($Fe_2O_3F_x$), because this would imply a partial oxidation of the Fe cations from 3+ in maghemite to 4+, to counteract the additional negative charge. An oxidation of iron from 3+ to 4+, though not impossible, seems unlikely. Substitution of one fluoride for one oxide anion would imply a partial reduction of iron from 3+ to 2+ to counterbalance the loss of negative charge.

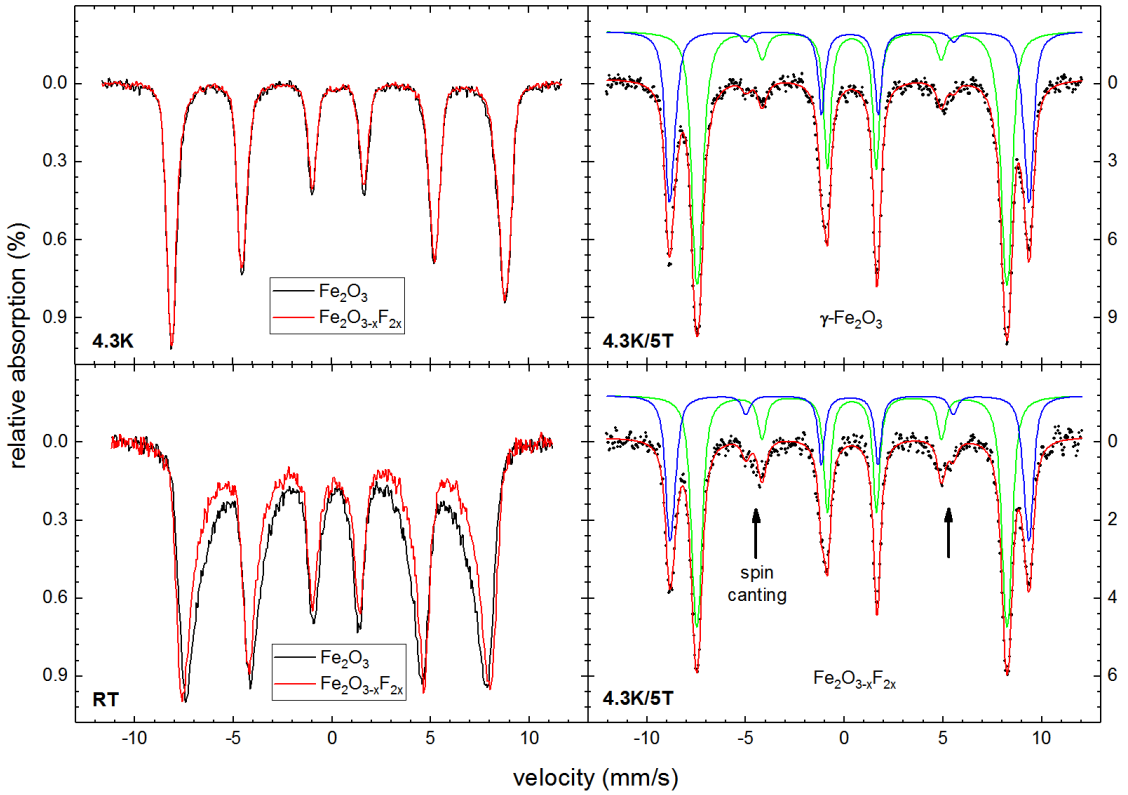

Figure 3- Mössbauer spectra of Fe_2O_3 and $Fe_2O_{3-x}F_{2x}$ nanoparticles recorded at 4.3K (top left), room temperature (bottom left), and at 4.3K in an external field of 5T along the γ-ray propagation direction (right, top and bottom). Spectra recorded without external magnetic field are directly compared for Fe_2O_3 (black) and $Fe_2O_{3-x}F_{2x}$ (red), while for the in-field spectra, individual subspectra of Fe^{3+} on A- (tetrahedral, blue) and B-sites (octahedral, green) can be identified.

Mössbauer spectra recorded at room temperature (RT), 4.3K, and at 4.3K under a magnetic field of 5T parallel to the γ-ray propagation direction are displayed in Figure 3. To make comparisons easier, the spectra at 4.3K and RT are superimposed, with no differences being visible at 4.3K, showing that no considerable changes in magnetic structure or Fe valence state have been caused by the fluorination, and that no secondary iron-bearing phases have formed. Both samples display a clear sextet spectrum, composed of the superposition of the two sub-spectra of A- and B-sites, as discussed below in detail, showing complete magnetic ordering. The RT spectra show a slight deviation between the two samples, mostly visible at the inner flanks, pointing towards beginning superparamagnetic relaxation.[28,29,30] As the HREM analysis will show, the particle size of both samples is fairly identical, which indicates that this slight difference in relaxation behaviour is mostly caused by the fluorine doping. The spectra recorded at 5T and 4.3K are shown separately. We can see two clearly resolved sub-spectra for the tetrahedral (A) and octahedral (B) Fe^{3+} sites. For ferrite systems, the presence of Fe^{2+} would lead to the observation of additional spectral contributions with higher isomer shift and lower hyperfine magnetic field, which were not observed in any of the described spectra.[31,32] The lack of Fe^{2+} indicates that the 1:1 = F:O substitution, i.e. the formation of an oxide-fluoride of general composition $Fe_2O_{3-x}F_x$ is an unlikely outcome, although it cannot be completely discarded. Substitution of two fluoride for one oxide anion ($Fe_2O_{3-x}F_{2x}$) seems the most likely scenario, which is also supported by the small increase in lattice parameters calculated from the PXRD data (from 8.344(2) Å in γ-Fe_2O_3 to 8.355(1) Å in fluorinated γ-Fe_2O_3). This scenario is also in agreement with the findings by Zhou et al., who carried out direct fluorination of γ-Fe_2O_3 nanoparticles under fluorine gas using a fluidized bed reactor. At reaction temperatures up to 250 °C, a phase of general composition $Fe_2O_{3-x}F_{2x}$ ($x < 1$) was obtained on the surface of the nanoparticle. The PXRD patterns for the products of this fluorination process are comparable with those we obtained, as they show that the fluorinated product maintain the γ-Fe_2O_3 structure, there are no impurities and no noticeable shift of the diffraction peaks.[13]

The 5T Mössbauer spectra show no significant change in the degree of inversion, with the ratio of spectral areas of the two Fe^{3+} subspectra remaining mostly unchanged for both samples. However, a clear difference can be observed in the relative intensities of lines 2 and 5, from which the degree of spin alignment or spin canting, respectively, can be inferred. As the particle sizes have been determined to be very similar for the two samples, the distinctly higher intensity of lines 2 and 5 in the spectrum of the $Fe_2O_{3-x}F_{2x}$ can presumably be explained by this sample showing a higher degree of spin canting. From experimental spectra, average spin canting

angles of ~24° ($Fe_2O_{3-x}F_{2x}$) and ~17° (Fe_2O_3) have been extracted. The higher spin canting may be explained in terms of an enhanced magnetic anisotropy as a result of fluorination.

To crosscheck this claim further, magnetometry measurements were performed on both samples, with Figure 4 showing a close-up of M(H) measurements performed up to maximum fields of 9T at 4.3K and RT, as well as M(T) zero field cooled – field cooled (ZFC-FC) measurements recorded between 5K and 350K at an applied field of 10mT. The 9T magnetization is decreased by 6% for the fluorinated sample compared to the undoped material, presumably due to the increased spin canting that was observed in the 5T Mössbauer spectra. However, the fluorinated sample also shows a coercive field that is twice as large as that of the undoped sample, also pointing towards a higher magnetic anisotropy constant. Furthermore, temperature dependent measurements reveal a larger splitting between FC and ZFC-magnetization curves, indicating overall lower blocking temperatures, i.e. lower magnetic anisotropy energy barriers, further substantiating this assumption.

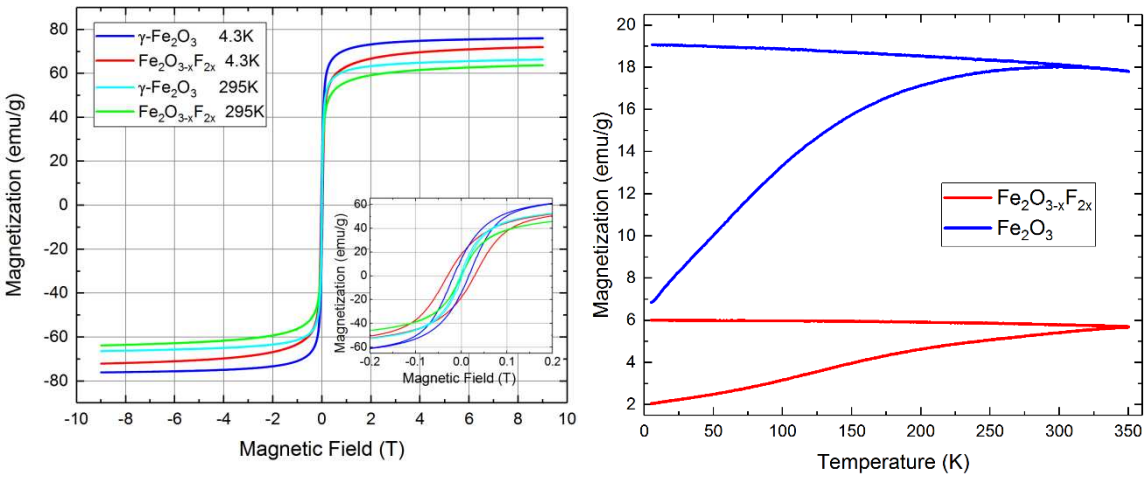

Figure 4- M(H) curves of Fe_2O_3 and $Fe_2O_{3-x}F_{2x}$ nanoparticles (left) up to a maximum field of 9T, recorded at room temperature and 4.3K, with the inset showing a close-up of the small field region. M(T) curves (right) of the same samples were recorded in a magnetic field of 10mT.

HREM images of γ-Fe_2O_3 and fluorinated γ-Fe_2O_3 nanoparticles are shown in Figure 5 with 5a and 5c representative of the size dispersion while 5b and 5d show an enlargement of a single particle lying in the 011 projection. From the comparison, it is apparent that there is no appreciable difference in morphology and size between the γ-Fe_2O_3 and fluorinated γ-Fe_2O_3

nanoparticles. Manual measurements carried out on several HREM images of the γ-Fe_2O_3 and fluorinated γ-Fe_2O_3 nanoparticles and the average size of both sets was found to be 10-12 nm.

The particle size was also estimated using the Scherrer equation, and found to be very similar for the two compounds, approximately 13.1 nm.

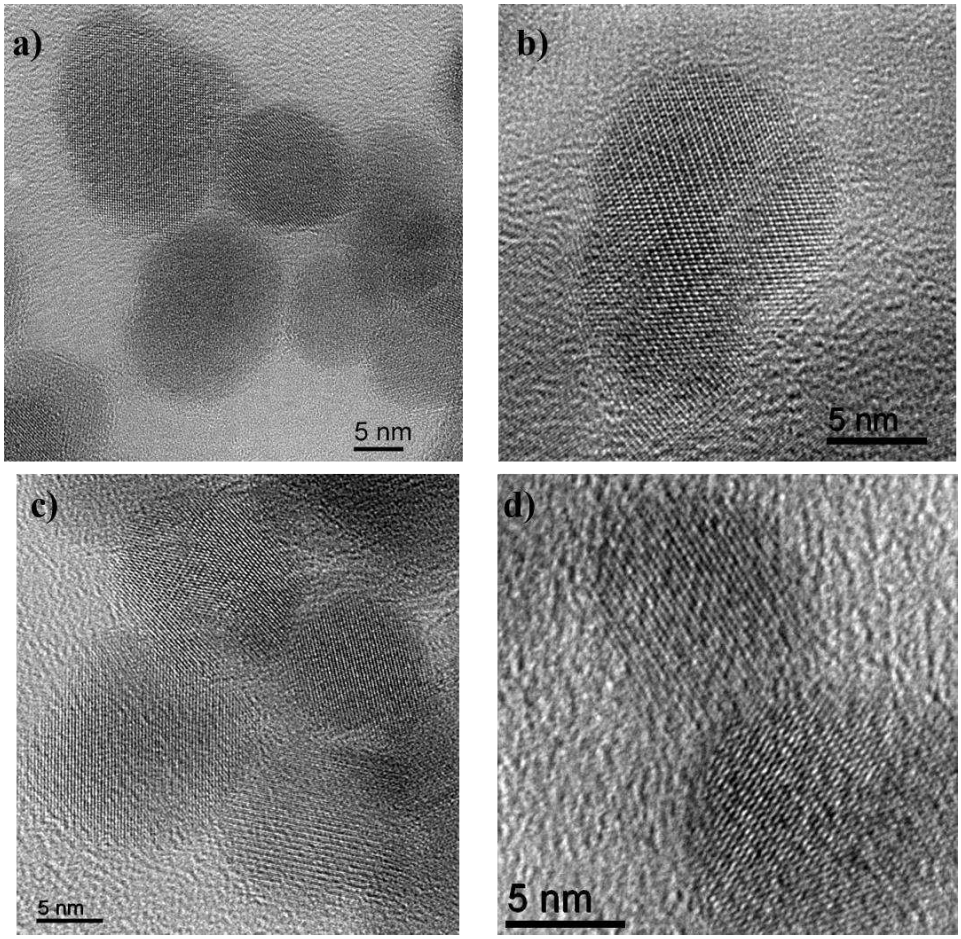

Figure 5 - HREM images of γ-Fe_2O_3, a) and b), and fluorinated γ-Fe_2O_3 nanoparticles, c) and d)

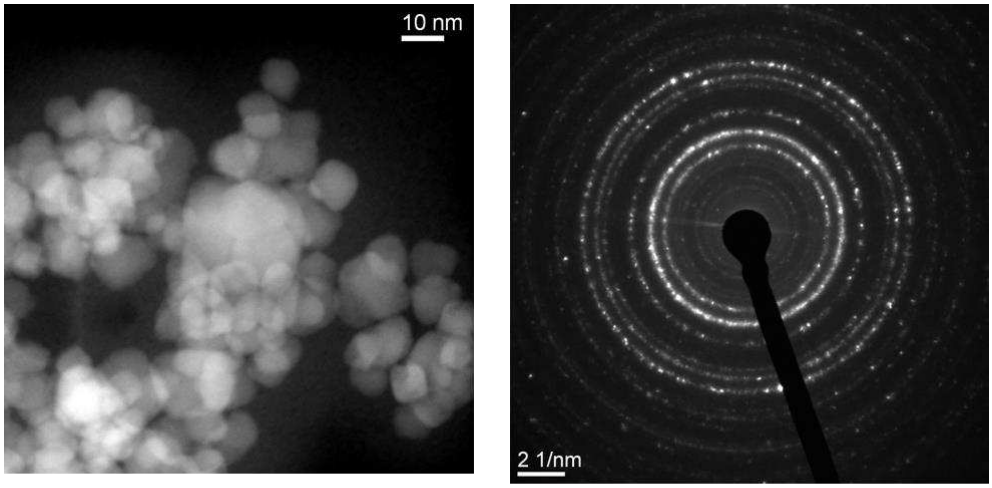

Figure 6. a) Large area image of uncoated fluorinated γ-Fe_2O_3 nanoparticles by HAADF-STEM imaging mode (Z-contrast). b) Typical diffraction pattern taken on an agglomerate.

Figure 6a shows that the nanoparticles tend to agglomerate, and this makes crystallographic studies on single particles a little difficult. Figure 6b shows a typical diffraction pattern taken on an agglomerate. The d spacings measured from the diffraction rings correspond to the lattice of the maghemite phase, confirming that the maghemite crystal structure is maintained after fluorination, as found by PXRD.

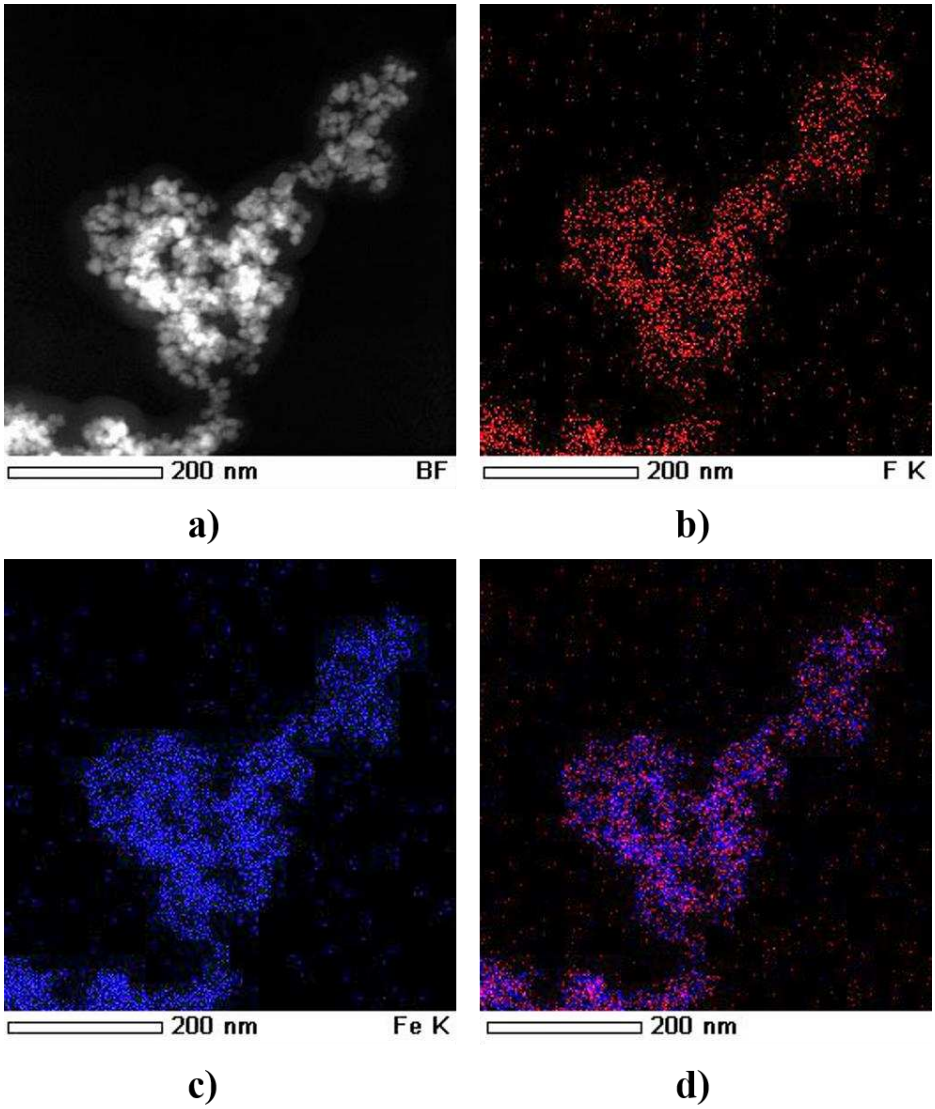

Figure 7. a) HAADF-STEM image of an agglomerate of fluorinated γ-Fe_2O_3 nanoparticles, b) X-ray map obtained by using the F K line (in red), c) X-ray map obtained by using the Fe K line (in blue), d) Map obtained by the overlapping of the two individual maps

Figure 7 shows elemental maps for the fluorinated γ-Fe_2O_3 nanoparticles and provides an indication that the distribution of iron and fluorine is homogeneous across the sample.

In order to determine the efficacy of the prepared nanoparticles as MRI contrast agents, MR measurements were carried out at magnetic field strengths of 11.7 T and 3 T. Current standard clinical MRI scanners use magnetic field strengths up to 3T, however further development of the technology may result in scanners utilising much higher magnetic field strengths for routine use in the future. With this in mind it is prudent to study the relaxation properties of the

prepared nanoparticles at both clinical field strengths and higher magnetic field strengths, in order to determine fully the potential of our new fluorinated γ-Fe_2O_3 as MRI contrast agent.

γ-Fe_2O_3 nanoparticles and fluorinated γ-Fe_2O_3 nanoparticles were coated with citric acid to create stable water suspensions and study the effects of fluoride doping upon the relaxivity. The data were subsequently compared against each other.

For γ-Fe_2O_3 nanoparticles at 3 T, r_1 = 0.522 $mM^{-1}s^{-1}$ and r_2 = 8.14 $mM^{-1}s^{-1}$. In comparison, for the doped γ-Fe_2O_3 nanoparticles at 3 T, r_1 = 1.74 $mM^{-1}s^{-1}$ and r_2 = 137 $mM^{-1}s^{-1}$. The new $Fe_2O_{3-x}F_{2x}$ nanoparticles show a 3-fold increase in r_1 relaxivity in comparison to γ-Fe_2O_3 nanoparticles, but more significantly, they show a 17-fold increase in the r_2 relaxivity. In addition, at 11.7 T γ-Fe_2O_3 nanoparticles exhibited r_1 = 3.19 $mM^{-1}s^{-1}$ and r_2 = 11.4 $mM^{-1}s^{-1}$, greatly icreased upon by the doped γ-Fe_2O_3 nanoparticles with an r_1 = 18.8 $mM^{-1}s^{-1}$, almost a 6-fold increase, and an r_2 = 167 $mM^{-1}s^{-1}$, a 14-fold increase. For current clinical imaging applications, lower field strengths of 1.5 to 3 T are standard. Hence, it is important to measure values at multiple field strengths, although, the higher field will provide improved T_2 relaxivity (r_2). The values observed in this study are low to average for γ-Fe_2O_3 nanoparticles as would be expected when the size and coating have not yet been optimised. Specifically, the synthetic route to prepare γ-Fe_2O_3 nanoparticles did not include any templating agent that would have assure maximum homogeneity in the size of the particle. The reason for this choice is the focus of this work on the purity of the γ-Fe_2O_3 phase to be used as starting material for fluorination, hence the exclusion of any additional factor that could have led to a sizeable presence of Fe_3O_4, as it often occurs. Typical values for previously published and clinically approved NPs are between 100-350 $mM^{-1}s^{-1}$.[33] The key point is the dramatic difference on fluoride doping of the material which has two major impacts: a 14 fold increase in the relaxivity versus the control nanoparticles and also a significant variation in the r_2/r_1 ratio which indicates a pure T_2 contrast agent. The next stage will be to produce smaller nanoparticles and observe the influence on T_1 relaxivity parameters. The optimisation of coating should further improve the properties. An optimised fluoride doped iron oxide nanoparticle is likely to have significant increased value for in vivo imaging and forms the next stage of this study.

Tube-in-tube MR images relative to water are shown in Figure 8.

(a)

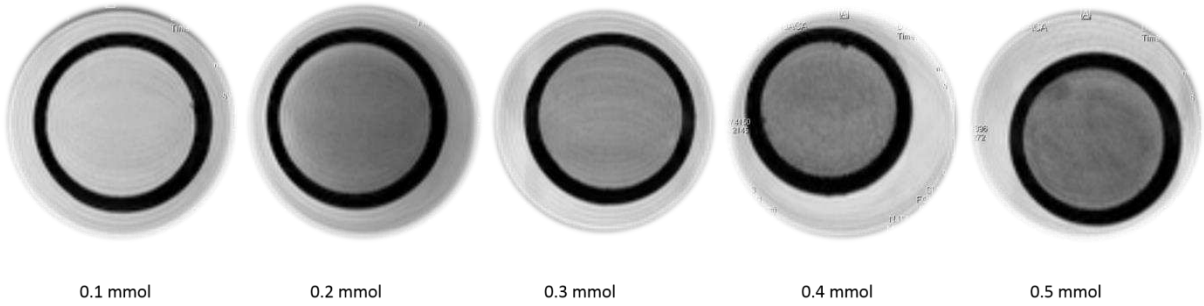

(b)

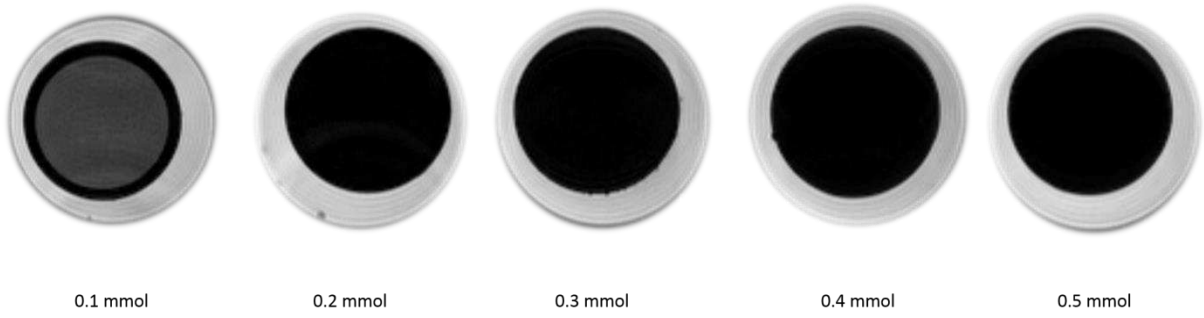

Figure 8 MRI T2 phantom images of aqueous solutions of γ-Fe_2O_3 (a) and $Fe_2O_{3-x}F_{2x}$ (b) nanoparticles at different concentrations.

Figure 8a shows that, at low concentrations (i.e. 0.1 mmol) there is little difference in relaxivity between the solution containing γ-Fe_2O_3 and the surrounding water, as shown by the similarity of contrast in both areas of the image. As the concentration on γ-Fe_2O_3 in the inner solution increases, the contrast becomes more negative (darker) showing an increase in the T2 relaxivity of the γ-Fe_2O_3 solution compared to water.

The comparison between Figure 8a and 8b shows an interesting insight. At 0.1mmol concentration, the difference in contrast between the suspension of $Fe_2O_{3-x}F_{2x}$ nanoparticles and the surrounding water is far more evident than the contrast between the suspension of γ-

Fe_2O_3 nanoparticles and the surrounding water. This indicates that even at low concentrations $Fe_2O_{3-x}F_{2x}$ may be, potentially, a more effective T2 contrast agent. The images show an increase in contrast as the concentration of $Fe_2O_{3-x}F_{2x}$ increases.

Conclusions

IONs (γ-Fe_2O_3 or Fe_3O_4 nanoparticles) are being heavily investigated for their potential as MRI contrast agents due to their high biocompatibility in comparison to other magnetic compounds, their high magnetic moment, low toxicity and wide availability. We prepared almost single-phase γ-Fe_2O_3 nanoparticles (98.5 % γ-Fe_2O_3 and 1.5% Fe_3O_4 in weight) via a co-precipitation method and subsequently carried out fluoride doping using a simple and low-cost methodology. Large increases in both r_1 and r_2 relaxivities are found in the fluorinated nanoparticles, in comparison to the bare γ-Fe_2O_3 nanoparticles. The PXRD patterns do not show any difference between the γ-Fe_2O_3 nanoparticles and their fluorinated counterparts, indicating that fluorination does not lead to any changes in crystal structure. The Mössbauer spectra reveal that the oxidation state of iron is unchanged, following fluorination, hinting that a possible general formula for this material may be $Fe_2O_{3-x}F_{2x}$. HREM shows that the particle size is unaffected by fluorination and STEM shows a homogeneous distribution of the fluorine throughout the sample in the doped nanoparticles. However, Mössbauer spectra at 5T magnetic field show a higher degree of spin canting in the fluorinated material, supporting results from the magnetic measurements, which show a largely enhanced coercive field and a higher magnetic anisotropy. Therefore, the large increase in the relaxivities seems to be solely due to the increased magnetic anisotropy, which may be related to an increased ionicity of the Fe-F bonds compared to the Fe-O bonds. However, the substitution of two fluoride anions for one oxide anions may also lead to a stronger hydrogen bonding between the fluoride anion and the surrounding water molecules, hence inducing changes in the relaxivities of the protons. These findings could open up possibilities of manipulating the magnetic anisotropy by performing substitutions that change the nature of the chemical bonds in nanoparticles.

1. R. Qiao, C. Yang, and M. Gao, J. Mater. Chem., 2009, **19**, 6274.

2. R. Hufschmid, H. Arami, R. M. Ferguson, M. Gonzales, E. Teeman, L. N. Brush, N. D. Browning, and K. M. Krishnan, Nanoscale, 2015, **7**, 11142–11154.

3. D. K. Kim, M. Mikhaylova, Y. Zhang, and M. Muhammed, Chem. Mater., 2003, **15**, 1617–1627.

4. K. K. Koenig SH1, Magn. Reson. Med., 1995, **34**, 227–33.

5. A. Figuerola, R. Di Corato, L. Manna, and T. Pellegrino, Pharmacol. Res., 2010, **62**, 126–143.

6. W. Feitknecht, Rev. Pure Appl. Chem, 1964, 423 – 440.

7. C. Bárcena, A. K. Sra, G. S. Chaubey, C. Khemtong, J. P. Liu, and J. Gao, Chem. Commun. (Camb)., 2008, 2224–6.

8. H. Yang, C. Zhang, X. Shi, H. Hu, X. Du, Y. Fang, Y. Ma, H. Wu, and S. Yang, Biomaterials, 2010, **31**, 3667–3673.

9. C. Hu, Z. Gao, and X. Yang, J. Magn. Magn. Mater., 2008, **320**, L70–L73.

10. M. G. Francesconi, M. G. Barker, P. a. Cooke, and A. J. Blake, J. Chem. Soc. Dalt. Trans., 2000, 1709–1713.

11. C. Greaves and M. G. Francesconi, Curr. Opin. Solid State Mater. Sci., 1998, **3**, 132–136.

12. J. P. and P. H. J. Claverie, L. Lozano, J. P. Odile, J. Fluor. Chem., 1974, **4**, 57–63.

13. H. Zhou, J. Nanda, S. K. Martha, J. Adcock, J. C. Idrobo, L. Baggetto, G. M. Veith, S. Dai, S. Pannala, and N. J. Dudney, J. Phys. Chem. Lett., 2013, **4**, 3798–3805.

14. H. Zhou, R. E. Ruther, J. Adcock, W. Zhou, S. Dai, and J. Nanda, ACS Nano, 2015, **9**, 2530–2539.

15. H.-Y. Lee, Z. Li, K. Chen, A. R. Hsu, C. Xu, J. Xie, S. Sun, and X. Chen, J. Nucl. Med., 2008, **49**, 1371–1379.

16. M. D. Normandin, H. Yuan, M. Q. Wilks, H. H. Chen, J. M. Kinsella, H. Cho, N. J. Guehl, N. Absi-Halabi, S. M. Hosseini, G. El Fakhri, D. E. Sosnovik, and L. Josephson, Angew. Chemie - Int. Ed., 2015, **54**, 13002–13006.

17. B. P. Burke, N. Baghdadi, A. E. Kownacka, S. Nigam, G. S. Clemente, M. M. Al-Yassiry, J. Domarkas, M. Lorch, M. Pickles, P. Gibbs, R. Tripier, C. Cawthorne, and S. J. Archibald, Nanoscale, 2015, **7**, 14889–14896.

18. B. P. Burke, N. Baghdadi, G. S. Clemente, N. Camus, A. Guillou, A. E. Kownacka, J. Domarkas, Z. Halime, R. Tripier, and S. J. Archibald, Faraday Discuss., 2014, **175**, 59–71.

19. J. Cheon and J. H. Lee, Acc. Chem. Res., 2008, **41**, 1630–1640.

20. R. T. M. De Rosales, J. Label. Compd. Radiopharm., 2014, **57**, 298–303.

21. D. A. Torigian, H. Zaidi, T. C. Kwee, B. Saboury, J. K. Udupa, Z.-H. Cho, and A. Alavi, Radiology, 2013, **267**, 26–44.

22. M. G. Francesconi, P. R. Slater, J. P. Hodges, C. Greaves, P. P. Edwards, and M. Slaski, J. Solid State Chem., 1998, **27**, 17–27.

23. M. G. Francesconi and C. Greaves, Supercond. Sci. Technol., 1997, **10**, A29–A37.

24. W. Kim, C. Y. Suh, S. W. Cho, K. M. Roh, H. Kwon, K. Song, and I. J. Shon, Talanta, 2012, **94**, 348–352.

25. C. Pecharroman, T. Gonzalezcarreno, and J. E. Iglesias, Phys. Chem. Miner., 1995, **22**, 21–29.

26. B. V. Crist, Handbook of Monochromatic XPS Spectra, The Elements of Native Oxides, Wiley, 2000.

27. A. P. Grosvenor, B. A. Kobe, M. C. Biesinger, and N. S. McIntyre, Surf. Interface Anal., 2004, **36**, 1564–1574.

28. G. F. Goya, T. S. Berquó, F. C. Fonseca, and M. P. Morales, J. Appl. Phys., 2003, **94**, 3520–3528.

29. K. Lefmann, F. Bødker, S. N. Klausen, S. Mørup, D. E. Madsen, C. Frandsen, D. E. Madsen, L. Cervera-Gontard, T. Kasama, H. Topsøe, B. S. Clausen, E. L. Duarte, R. Itri, E. Lima, M. F. Hansen, C. B. Koch, D. Predoi, V. Kuncser, E. Tronc, E. Brok, and C. Frandsen, 2000.

30. J. Landers, F. Stromberg, M. Darbandi, C. Schöppner, W. Keune, and H. Wende, J. Phys. Condens. Matter, 2015, **27**.

31. R. S. Hargrove and W. Kündig, Solid State Commun., 1970, **8**, 303.

32. M. Darbandi, F. Stromberg, J. Landers, N. Reckers, B. Sanyal, W. Keune, and H. Wende, J. Phys. D. Appl. Phys., 2012, **45**.

33. S. Laurent, D. Forge, M. Port, a Roch, C. Robic, L. V Elst, and R. N. Muller, Chem. Rev., 2008, **108**, 2064–2110.